

1 **POROSIMETRIC CHARACTERIZATION OF POLYSULPHONE**
2 **ULTRAFILTRATION MEMBRANES BY IMAGE ANALISYS AND**
3 **LIQUID-LIQUID DISPLACEMENT TECHNIQUE.**
4
5
6

7 **José Ignacio Calvo^{1,†}, René Israel Peinador¹, Pedro Prádanos¹, Aldo Bottino², Antonio**
8 **Comite², Raffaella Firpo² and Antonio Hernández¹**
9

10 **¹ Surfaces and Porous Materials Group (SMAP), UA-UVA-CSIC, University of Valladolid,**
11 **47071 Valladolid, Spain**

12 **² Department of Chemistry and Industrial Chemistry, University of Genoa, Vía Dodecaneso,**
13 **16141 Genoa, Italy**
14
15

16
17
18 **ABSTRACT**
19
20
21

22 Structural and surface properties of two commercial polysulfone ultrafiltration membranes
23 have been evaluated by different techniques. Pore size distributions have been determined by
24 Liquid-Liquid Displacement Porosimetry (LLDP) as well as by image analysis performed onto
25 Field Emission Scanning Electron Microscopy (FESEM) images of the membrane surfaces. Fourier
26 Transform Infrared Spectroscopy (FTIR) has been used to investigate membrane composition, and
27 in particular, to obtain proper information on the presence of additive within the membrane
28 structure.
29
30

31 Porosimetric results obtained by the two independent techniques compared reasonably well
32 and the Molecular Weight Cut Off (MWCO) of the two membranes estimated from LLDP pore size
33 distribution were found to be in good agreement with the nominal values given by manufacturers.
34
35
36
37
38

39 **KEYWORDS:**
40

41 Ultrafiltration, Pore size distribution, Liquid-Liquid Displacement Porosimetry, Electron
42 Microscopy, Molecular Weight Cut-Off.
43
44
45
46
47
48
49
50
51
52
53

54 † To whom correspondence should be addressed. jicalvo@termo.uva.es
55
56
57
58
59
60
61
62
63
64
65

INTRODUCTION

Ultrafiltration (UF) is a pressure driven process where membranes are used to separate macromolecules from fluid streams. In such process, the selectivity is mainly determined by the porous structure, since retention is determined for these membranes by a sieving mechanism.

In that sense, sieving curves are the usual way to evaluate the selectivity of UF membranes. These curves are obtained plotting the retention of some selected solutes, called tracers, versus their molecular mass and analysis of such plots lead to define the so-called Molecular Weight Cut-Off (MWCO), a key parameter in selecting membranes for given applications. This parameter has reached the category of a “de facto” standard, [1], for the characterization of UF membranes, but also for nanofiltration (NF) ones, [2].

In effect, for membrane manufacturers and end-users as well, MWCO value is a very valuable parameter because it gives an idea about the molecular weight of species being separated by such membrane.

Manufacturers generally specify for their membranes a nominal MWCO defined as the molecular mass of the solute that is (or would be) 90% retained by the membrane. However, it has been often pointed out, [3–8], that the reported values of cut-off for a given membrane may be strongly dependent on the different methodologies and/or experimental test conditions used. Effectively, the influence of important experimental factors as, for example, device configuration and operational parameters as channel geometry or feed turbulence degree on the membrane surface, which prevent concentration polarization and fouling phenomena, are quite often neglected. Moreover, these factors are not always controlled or clearly stated, [1].

Moreover the results of retention tests cannot be really considered as a characteristic parameter of the membrane because they also depend on the shape, flexibility and molecular weight distribution of the macromolecules used for these tests, [9], and their interaction with the membrane materials. So, it can be concluded that the results from retention tests could be sometimes far from what might be expected from the actual membrane pore size, [10].

Another aim when determining MWCO is to evaluate the pore size distribution of membranes in order to know, from such structural information, which molecules can be retained or passed through the membrane pores. Once a unique relationship between retention results and the actual structural characterization of the membrane is assumed, the knowledge of the actual structure of the pores in the membrane will be really informative because it could be translated into retention characteristics for each particular solute.

Many characterization methods like permporometry, thermoporometry, mercury porosimetry, gas adsorption-desorption, nuclear magnetic resonance, gas-liquid and liquid-liquid porosimetry along with several microscopic techniques, both electronic as scanning and transmission electron microscopy and atomic as atomic force microscopy, have been used to analyze the pore structure and pore size distribution of the membrane, [11]. Each of these methods has different features, principles of operation and need different theoretical considerations to convert the direct results into pore sizes. In any case, the information given by all these methods must not be considered as competitive but rather complementary, since all results should contribute to a complete picture of the pore characteristics.

UF membranes usually present pores in the range from some nanometers to 50 nanometers (0.05 μm) and a proper knowledge of the size distribution of those pores actually open for the flux

(active pores) is of great interest to estimate the sort of macromolecules retained. Techniques, such as those based on the bubble point test that have gained enormous relevance for the characterization of microfiltration membranes, cannot be properly applied to UF membranes due to the high pressure (more than 10 bar) to be applied in order to evaluate pore sizes below 0.1 μm , owing to the high value of the surface tension ($\gamma = 72 \text{ mN/m}$) between air and the wetting liquid (water), [11]. On the contrary Liquid-Liquid Displacement Porosimetry (LLDP), because it uses a pair of immiscible liquids with very low interfacial tension is very suitable for characterizing UF membranes at relatively low applied pressures. Tung et al., [12], consider the technique as relatively new although, in fact, it comes from earlier works of Erbe, [13], who proposed the principles of the methodology as an extension of the well-known bubble point technique previously proposed by Bechhold, [14]. After several years of scant attention; in recent times, more and more research groups are getting interesting results using LLDP for the characterization of ultrafiltration membranes, [15-18].

Some of us in the frame of a long-term collaboration, have designed and built-up powerful LLDP devices, fully automated and very precise, for obtaining an exhaustive porosimetric characterization of UF membrane with different MWCO and configuration, [19-25].

In this work, porosity and pore size distribution of two different kinds of commercial polymeric UF membranes evaluated by LLDP will be used to estimate their MWCO according to a procedure previously developed, [26].

In addition to LLDP experiments, FESEM pictures will be obtained and used to get information on pore size distributions. Image analysis of several microscopic images is frequently used because it gives a good view of the membrane surface that can be used to study surface membrane modifications, [27-29]. In this case such image analysis was performed in order to obtain independent information on the porosimetric characteristics of the membrane.

Finally FTIR combined with Attenuated Total Reflectance (ATR) and Photoacoustic Spectroscopy (PAS), allows analyzing the membrane composition and provides an useful help for a better understanding of some anomalous results we obtained at the initial steps of LLDP measurements.

EXPERIMENTAL

Membranes and Chemicals

Two commercial UF membranes (GR61PP and GR70PE) were kindly supplied by Alfa-Laval. Both membranes are made from polysulphone and have a MWCO of 20 kDa, according to the manufacturer, [30].

All membrane discs were bathed in Milli-Q water for 24 hours to eliminate any previous soaking of preservative agent, before being used for LLDP analysis.

Isobutanol from Scharlab (analysis grade, purity > 99,5 %) was used as received without further purification. Water was bidistilled and Milli-Q treated freshly prior to use.

Liquid-liquid Displacement Porosimetry

The porosimeters used in the analysis consist in two twin automated devices developed in parallel in SMAP (University of Valladolid) and DCCI (University of Genoa) laboratories, [19, 20].

A detailed description of the equipment and the experimental procedure can be seen elsewhere, [20], while a scheme of the experimental setup has been published in several previous papers, see for example, [26]. The main feature of the equipment is the use of a precise syringe pump ISCO-250D, allowing accurate and very stable fluxes without fluctuations that make unnecessary any sort of dampening. The experimental procedure allows relating the applied pressure and the corresponding pore radius opened at a given applied pressure according to the Cantor equation, [31], provided that the contact angle between the liquid-liquid interface and the membrane material could be assumed to be zero,

$$\Delta p = \frac{2\gamma}{r_p} \quad (1)$$

where Δp is the applied pressure, γ the interfacial tension (1,9 mN/m in our experimental conditions) and r_p the equivalent pore radius.

By increasing the applied pressure stepwise, corresponding pore radii and flux values, represented as the permeability of the membrane (flux/pressure ratio), are obtained and form what we call porogram. Therefore, by measuring the equilibrium pressure drop corresponding to each increment of flux, a pore size distribution of the membrane can be evaluated.

For that it is supposed pores are cylindrical and normal, then Hage-Poiseuille equation for convective flow applies to correlate the volumetric flow, F , and the number of pores, n_k , having a pore radius, r_k . For each pressure step, p_i , the corresponding flow measured, F_i , can be correlated in such a way with the number of pores opened in that and all previous steps by:

$$F_i = \sum_{k=1}^i \frac{n_k \pi r_k^4}{8\eta l} p_i \quad (2)$$

where η is the dynamic viscosity of the displacing fluid (aqueous phase of liquid mixture, then a value of 0.89 mPa·s, for water at 25 °C, was used in calculations), l is the pore length (membrane thickness for symmetric membranes while for asymmetric ones must be evaluated as the active layer thickness). n_k and r_k are, respectively, the number of pores and the radius of such pores opened up during the k -th step (for $k = 1, \dots, i$).

It should be noted that this pore size corresponds to the narrowest section along the pore found across the whole membrane. Even with membranes having a so complicated pore structure (hourglass like) as those here studied, this technique focuses in the part of the pores which presents the narrowest section. This section is what effectively governs fluid transport and also retention capabilities.

The liquid mixture used to perform the LLDP measurements has been a 1:1 w/w mixture of water/isobutanol. The mixtures were prepared by pouring proper amounts of Milli-Q grade water and alcohol into a separator funnel and shaking it vigorously. The mixtures were then allowed to stand overnight. The separated alcohol-rich phase was drained off and used as the wetting liquid and the aqueous-rich phase was used as the displacing liquid.

Previous tests on different membranes showed that using isobutanol for wetting led frequently to better results as compared with analysis in which water phase was used for wetting and alcoholic one pushed out the other phase. In any case this possibility of choosing among both liquids which one acts as wetting phase and which one as pushing liquid, is one of the interesting

1 features of LLDP, [23], and would be determined by the interaction of the wetting phase with the
2 membrane active layer material.

3 Wet samples were then placed in the measurement cell and aqueous phase was used to push
4 out the wetting liquid.
5

6 **Cut-Off Estimation**

7 LLDP offers a simple and fast method to estimate cut-off molecular weight for UF
8 membranes. In order to perform such estimation, it is necessary to complete the LLDP to get the
9 number pore size distribution. This distribution can be presented as cumulative, i.e. plotting the
10 number of pores with radii below each given pore size. In such a representation the biggest pore
11 corresponds to the first one opened while the smallest one should be opened when the 100% of the
12 flux has been reached. A graphical determination of the pore size such that 90 % of the pores are
13 smaller, and only 10 % of the total pores are bigger, should define what we will use to estimate the
14 molecular weight cut-off for the membrane, [26]. In this estimation, a semiempirical correlation
15 between molecular weight, diffusion coefficient and molecule Stoke's radius, valid for dextran
16 molecules, [32], will be used.
17

18 This approach relates the diffusion coefficient of dextran molecules at infinite dilution in
19 water, D_∞ , to the molecular weight of the dextran (M) as follows:
20

$$21 \log D_\infty = -4.1154 - 0.47752 \log(M) \quad (3)$$

22 From this value, the Stoke radius of the dextran molecule can be obtained with the well
23 known equation:
24

$$25 r_s = \frac{k_B T}{6\pi\eta D_\infty} \quad (4)$$

26 being k_B the Boltzmann's constant, T the absolute temperature and η the water viscosity at such
27 temperature.
28

29 Using this approach, the MWCO, corresponding to the pore size with 90 % of the smaller
30 pores, can be determined. Obviously this estimation is based on pseudo-empirical molecular-weight
31 versus size correlations for dextrans. Similar correlations can be found for PEG's or other
32 molecules commonly used as tracers, giving slightly different cut-off estimation values.
33

34 **SEM Microscopy**

35 Two kinds of electron microscopes have been used. Firstly some membrane pieces, after
36 fracturation in liquid nitrogen, to give sharp cross sections, were viewed in a conventional Scanning
37 Electron Microscopy (SEM) apparatus (LEO Stereoscan 440). Samples were previously sputtered
38 with a thin layer of gold and then imaged to evaluate the active layer thickness which would be used
39 as input parameter in the porosimetric calculations.
40

41 Some other pieces of each membrane were top surface viewed in a FESEM equipment
42 (Zeiss Supra 40 VP), using a thin deposited layer of Chromium to increase contrast. Those images
43 were digitalized and analyzed using commercial Image Analysis software (ScanPro from Jandel),
44
45

able to count and measure all the pores present in the picture. Feret equivalent radii were determined by using this software and results were converted in a pore size distribution.

FTIR

FTIR (ATR and PAS) spectra were recorded by using a Bruker IFS66 spectrometer with 2 cm^{-1} resolution. Details on sampling technique and experimental procedure used for these type of measurements are reported elsewhere, [33].

RESULTS AND DISCUSSION

LLDP

A first series of LLDP measurements was carried out with membranes (after water bathing as previously described) by using the isobutanol phase as displacing liquid. However in the case of GR61PP this procedure did not lead to good results since the behavior of the flux vs. applied pressure appeared very peculiar and different from that found for the GR70PE membrane which presented a S-shape curve typical of displacing porosimetry, [11]. So, taking profit of the feature that both liquids can interchange their roles, a new series of measurements were done by using now the alcohol rich phase as wetting liquid. In this case the porosimetric curves coming from both membranes presented a similar S-shape. An example for such curves is presented for GR70PE (see Figure 1) with a nil flux up to achieve the minimum pressure necessary to overcome the interfacial forces inside the bigger pores. This initial flux can be matched with the bubble point of a bubble pressure measurement.

Figure 1

Using the raw porosimetric data of a given membrane sample, we can obtain the permeability distributions (Fig. 2) as the simple contribution of each pore size yet opened to the whole membrane permeability (in this case the ordinates axis has been shown as the percent of the final permeability of the sample).

Figure 2

Then using the Hagen-Poiseuille model for convective transport of fluid inside cylindrical parallel capillaries, we can convert the permeability distribution into a pore number distribution (Fig. 3), [26]. This figure presents the percentage of pores in each pore class which is needed to obtain the permeabilities shown in the previous figure (Fig. 2).

Figure 3

Clearly both pore-size distributions (from permeabilities and from pore numbers) along with others similarly based on a transport model, as for example, pore areas distribution, can be shown as cumulative values. Examples of such cumulative distributions are shown in Fig. 4 again for the GR70PE membrane. In this case we have shown permeability, area and pore number distributions together and it can be seen how all them show a clear shift to lower pore sizes when compared to the direct permeability data. The reason is related to the fourth power dependence of the flow rate with pore radius, according to Hagen-Poiseuille law, which means that a lot of small pores are needed to obtain the same permeability contribution given by a much lower amount of bigger pores.

1 Finally the area of the pores is proportional to the square of pore size, so the corresponding area
2 distribution relies between permeability and pore number ones.

3 **Figure 4**

4
5
6 The cumulative distribution of pore numbers can be used to get an estimation of the
7 molecular weight cut-off, MWCO, of the membranes. This procedure, as explained above, is based
8 on accounting for the pore size over 90 % of the whole pore population. This calculation is made
9 graphically with the aid of the dotted lines shown in Fig. 4.

10
11
12 Once the way to obtain the porosimetric information from typical LLDP experiments has
13 been described, in the following figures (Figs. 5 and 6) we are presenting the comparative results of
14 such porosimetric analysis for both the studied membranes. The figures present the porosimetric
15 runs for several samples made both in Genoa and Valladolid. It could be remarked the fair
16 agreement of the experimental data collected in both laboratories, especially as coming from not
17 commercial devices. Here, we have presented the size distribution as obtained from direct
18 permeability data, which is more reliable as does not need any transport model or structural
19 hypothesis which could result in a poor accordance with the actual membrane pattern. The resulting
20 pore size distributions are centered in values around 3 nm for GR61PP and roughly about 6 nm for
21 GR70PE (mean size for this membrane is lower since the sharp increase in the flux-pressure curves
22 happens at lower pressures, around 5 bars, as compared with that of GR61PP, with increasing flux
23 after achieving more than 10 bars). Finally pore size distributions for both membranes show nice
24 reproducibility as previously shown in LLDP analysis, [34].

25 **Figure 5**

26 **Figure 6**

27
28
29 The data conversion algorithm based, as commented previously, on applying the Hagen-
30 Poiseuille model for the transport inside the pores, needs a previous knowledge of the pore length
31 (which can be matched with the active layer thickness). To this aim, cross-sections of both
32 membranes were observed with a SEM to obtain an appraisal of such thicknesses. Figures 7a and 7b
33 show such cross-sectional images, for GR61PP and GR70PE, respectively. From those images it is
34 apparent that the active layer thickness of the first membrane is considerably lower. For our
35 calculations we assumed an average active layer thickness of 12 μm for GR61PP and 42 μm for
36 GR70PE, that approximately correspond to the distance between the membrane surface and the top
37 of the large cavities.

38
39
40 Regarding these values, it must be considered that, as it is well known, asymmetric
41 membranes present a continuous and gradual increase in the pore size from the top layer to the inner
42 of the membranes. Then it is very complicated to accurately define the pore length since it depends
43 not only on the skin layer thickness (which in turn is not so easy to determine) but also on the pore
44 tortuosity factor. In any case, the pore length affects the final values of porosity and pore density,
45 along with the absolute number of pores present in each class while has no effect on the relative
46 frequency of each pore size in the pore number distributions and the whole permeability
47 distribution, and, correspondingly, the mean pore sizes in each distribution.

48 **Figure 7**

1 The most representative data derived from the LLDP analysis (porosity, mean pore radius:
2 two values, from permeability and from pore number) for both GR membranes are reported in table
3 1, along with the estimated values of MWCO.

4
5 **Table 1**

6
7 **FTIR**

8
9 On the basis of the anomalous behavior observed at the beginning of the LLDP
10 measurements we decided to obtain a deeper information on the membrane composition with the
11 help of FTIR instrument by using the attenuated total reflection (ATR) technique in order to better
12 characterize the thin surface active layer of the membrane (which controls the membrane
13 performance) and to avoid any possible interference by the macroporous polyolefinic nonwoven
14 support. Moreover the PAS sampling technique was employed to obtain the spectra of the pure
15 components of the membrane. The ATR spectra of both membranes, analyzed as received (Fig. 8)
16 present a broad peak around 3600 and 3000 cm^{-1} (OH) along with a narrower one centered at 1030
17 cm^{-1} (CO) that, as the same figure reveals, practically disappears after bathing both membranes in
18 pure water.
19
20
21

22 **Figure 8**

23
24 A comparison of these spectra with that of glycerol reported in Fig. 9 allows ascribing the
25 disappeared peaks, to this type of polyalcohol—which is a common preservative added to the
26 polymeric membrane.
27

28 **Figure 9**

29
30 Further comparison of Figs. 8 and 9 allows concluding that both membranes are made of
31 polysulfone (PSF) as trunk material as demonstrate the absorption bands around 1150 cm^{-1} and
32 1295 cm^{-1} (SO₂), 1250 cm^{-1} and 1020 cm^{-1} (C-O), 1590 cm^{-1} and 1500 cm^{-1} (aromatic ring), [35].
33 However a more accurate inspection of the spectra of the GR70PE membrane reveals the presence
34 of a foreign component which can be ascribed to polyvinylpyrrolidone, PVP, as show (Fig. 9), the
35 absorption bands around 1667 cm^{-1} (amide carbonyl), 1220 cm^{-1} (C-N) and in the 1500-1350 cm^{-1}
36 region (Cyclic CH₂), [36]. It is worth remembering that PVP is often added to PSF in order to
37 prepare membranes with a better hydrophilic character, [37, 38]. On the basis of this finding it is
38 possible to conclude that the initial unreliable LLDP results obtained for GR61PP membrane are
39 due to the hydrophobic character of this type of PSF membrane that is not completely wetted upon
40 immersion in water as it occurs for the hydrophilic (PSF-PVP) GR70PE membrane. The spectra
41 shown in Fig. 10 clearly demonstrate that presence of PVP even after two consecutive LLDP
42 measurements.
43
44
45

46 **Figure 10**

47
48
49 **FESEM images**

50
51
52 Examples of the FESEM images obtained for top views of both membranes are presented in
53 Fig. 11. After a proper refining of the images (mainly increasing the contrast and definition of pore
54 borders, [39]) the resulting images were used to measure the size (Feret diameter) of the pores
55 present in the picture.
56

57
58 **Figure 11**

1 Resulting distributions are presented in Figs. 12a and 13a for both membranes, and main
2 parameters resulting from such distributions are also presented in table 1. In these figures, the
3 distribution of pore sizes obtained from image analysis are compared with that of number of pores
4 evaluated from LLDP data after modeling (an example of such number distributions is presented in
5 Fig. 3). We can see that image analysis and LLDP distributions are centered on quite similar values
6 of pore radius but those coming from FESEM images appear much broader. This is partially due to
7 the higher range of minimum pore sizes detectable with LLDP (around 2 nm at the maximum
8 applied pressures, while FESEM can apparently detect pores of 0.5 nm), but the major reason of
9 this disagreement is that FESEM images have lower resolution for these small pores leading to
10 confusion between actual pore entrances and simply darker areas of polymeric surface. Even so, the
11 accordance between mean pore sizes from both techniques is really reasonable, showing the
12 accuracy of the analysis done.
13
14

15 **Figure 12**

16
17
18 **Figure 13**
19
20
21
22

23 In any case, these pore number distributions can be used to estimate the MWCO of the
24 membranes, following the previously explained procedure, yet used for LLDP data. That estimation
25 is presented in Figs. 12b and 13b, where cumulative distributions of pores sizes for both membranes
26 are presented, some coming from LLDP data and the others as resulting from FESEM images
27 analysis. The microscopy results clearly would lead to an overestimation of MWCO, as can be
28 expected from their wide distribution.
29
30

31 This overestimation can be due firstly to the appearance of many small pores due to image
32 artifacts (shadows, surface defects...) that the software considers as real pores. Moreover big pores
33 are differently detected by both the techniques. Microscopy accounts for pore entrances, as seen in
34 the membrane surface, while LLDP only takes into account the smallest section of the pore across
35 the whole active layer.
36
37

38 Note that, as mentioned, the estimations coming from LLDP results are quite reasonable.
39 For the sake of comparison, single arrows mark in both membranes the MWCO corresponding to
40 the nominal value (as claimed by manufacturer) of both membranes, which is in turns equal. The
41 accordance between our estimations and the nominal values is really remarkable, showing the
42 power of LLDP characterization to give a complete picture not only about structural parameters of
43 analyzed membranes (mean pore size or porosity) but also giving a reasonable estimation of
44 performance related parameters, specially MWCO, a key parameter in terms of selection of
45 membranes for given applications.
46
47
48

49 Finally the values of porosity present in table 1 merit a brief comment. Those are largely the
50 worst values in terms of comparison, not only from LLDP to SEM outputs but also when coming
51 from different labs. In that sense, it must be remembered that, as commented previously, the
52 porosity results in the case of LLDP analysis are strongly affected by the values used for pore
53 length (assumed as active layer thickness, once zero tortuosity assumed). And this value, obtained
54 from SEM cross sectional images, is subjected to some uncertainty. On the other side, porosity
55 value coming from top view of FESEM images is affected by the image definition.
56
57
58

59 CONCLUSIONS

60
61
62
63
64
65

1 LLDP has been used to obtain the structural information of two commercial UF membranes.
2 This porosimetric technique supplied very precise and repetitive results which allowed to estimate
3 for both membranes a MWCO close to the one quoted by manufacturer.

4
5 Moreover, LLDP results have been compared with those coming from image analysis of
6 FESEM pictures. Taking into account that this later information refers only to membrane surface,
7 the mean pore sizes for both membranes match reasonably with those given from LLDP
8 characterization (which **accounts** not for surface opening but for the narrowest section of the pore
9 present across its way through the membrane). Nevertheless the agreement is not so good when
10 comparing MWCO estimations from both techniques. FESEM images lead to clear overestimation
11 of MWCO due to the presence of multiple pores and artifacts, difficult to avoid **when analyzing so**
12 **small pores very close to the maximum resolution of the technique**. This overestimation being also
13 related with the fact that FESEM only accounts for the pore entrance, while LLDP refers to the
14 narrowest section present across the pore length.
15
16

17
18 Finally the use of FTIR-ATR analysis allowed acquiring proper information on the
19 membrane composition, especially on the presence of additives which affect the membrane
20 wettability, thus providing an important help for defining the more appropriate way to carry out
21 LLDP measurements and obtain reliable data.
22

23 24 **ACKNOWLEDGEMENTS**

25
26 Alfa-Laval (Austria) is acknowledged for supplying membrane samples. Spanish authors
27 thank the Ministerio de Educación y Ciencia (Plan Nacional de I+D+i) through project CTQ2009-
28 07666 and Junta de Castilla y León (project VA-324A11-2), for funding of this research.
29
30

31 **REFERENCES**

- 32
33
34
35 1.- A.L. Zydney, A. Xenopoulos, Improving dextran tests for ultrafiltration membranes: Effect
36 of device format, *J. Membrane Sci.* 291 (2007) 180–190.
37
38 2.- B. Van der Bruggen, C. Vandecasteele, Modelling of the retention of uncharged molecules
39 with nanofiltration, *Water Res.* 36 (2002) 1360–1368.
40
41 3.- K.J. Kim, A.G. Fane, R. Ben Aim, M.G. Liu, G. Jonsson, I.C. Tessaro, A.P. Broek, D.
42 Bargeman, A comparative study of techniques used for porous membrane characterization: pore
43 characterization, *J. Membrane Sci.* 87 (1994) 35–46.
44
45 4.- P. Brown, Assessing the molecular weight cut-off value of UF membranes, *Membr.*
46 *Technol.* 61 (1995) 7–9.
47
48 5.- J.G. Jacangelo, S.S. Adham, J.M. Laîné, Mechanisms of cryptosporidium, giardia and MS2
49 virus removal by MF and UF, *J. AWWA* 7 (1995) 107–121.
50
51 6.- B. Schlichter, V. Mavrov, H. Chmiel, Comparative characterization of different commercial
52 UF membranes for drinking water production, *J. Water Supply: Res. Technol.-AQUA* 49.6 (2000)
53 321–328.
54
55 7.- S. Platt, M. Mauramo, S. Butylina, M. Nyström, Retention of pegs in cross-flow
56 ultrafiltration through membranes, *Desalination* 149 (2002) 417–422.
57
58
59
60
61
62
63
64
65

- 1 8.- A. Morão, M.T. Pessoa de Amorim, A.Lopes, I. Escobar, J.A. Queiroz, Characterisation of
2 ultrafiltration and nanofiltration membranes from rejections of neutral reference solutes using a
3 model of asymmetric pores, *J. Membrane Sci.*, 319 (2008) 64–75.
4
5
6 9.- M. Cheryan, *Ultrafiltration and Microfiltration Handbook*, Technomic Pub. Co. Inc.,
7 Lancaster, PA, USA, 1998.
8
9
10 10.- B. Chakrabarty, A.K. Ghoshal, M.K. Purkait, Effect of molecular weight of PEG on
11 membrane morphology and transport properties, *J. Membrane Sci.* 309 (2008) 209–221.
12
13 11.- J.I. Calvo, A. Bottino, P. Prádanos, L. Palacio, A. Hernández, Porosity, in: E.M.V. Hoek,
14 V.V. Tarabara (Eds.), *Encyclopedia of Membrane Science and Technology*, John Wiley and Sons,
15 Hoboken, NJ (USA), 2014.
16
17
18 12.- K.-L. Tung, K.-S. Chang, T.-T. Wu, N.-J. Lin, K.-R. Lee, J.-Y. Lai, Recent advances in the
19 characterization of membrane morphology, *Curr. Opin. Chem. Eng.*, 4 (2014) 121–127.
20
21
22 13.- F. Erbe, Blockierungsphenomene bei ultrafiltern, *Kolloid Z.*, 59 (1932)32–44.
23
24
25 14.- H. Bechhold, The permeability of ultrafilters, *Z. Phys. Chem.*, 64 (1908) 328–342.
26
27 15.- F. Shi, Y. Ma, J. Ma, P. Wang, W. Sun, Preparation and characterization of PVDF/TiO₂
28 hybrid membranes with ionic liquid modified nano-TiO₂ particles, *J. Membrane Sci.*, 427 (2013)
29 259–269.
30
31 16.- M.A. Masuelli, M. Grasselli, J. Marchese, N.A. Ochoa, Preparation, structural and
32 functional characterization of modified porous PVDF membranes by γ -irradiation, *J. Membrane*
33 *Sci.*, 389 (2012) 91– 98.
34
35
36 17.- M.K. Sinha, M.K. Purkait, Increase in hydrophilicity of polysulfone membrane using
37 polyethylene glycol methyl ether, *J. Membrane Sci.*, 437 (2013) 7–16.
38
39
40 18.- M.K. Sinha, M.K. Purkait, Preparation and characterization of novel pegylated hydrophilic
41 pH responsive polysulfone ultrafiltration membrane, *J. Membrane Sci.*, 464 (2014) 20–32.
42
43
44 19.- J.I. Calvo, A. Bottino, G. Capannelli, A. Hernández, Comparison of liquid-liquid
45 displacement porosimetry and scanning electron microscopy image analysis to characterise
46 ultrafiltration track-etched membranes, *J. Membrane Sci.* 239 (2004) 189–197.
47
48
49 20.- J.M. Sanz, D. Jardines, A. Bottino, G. Capannelli, A. Hernández, J.I. Calvo, Liquid-liquid
50 porometry for an accurate membrane characterization, *Desalination* 200 (2006) 195–197.
51
52
53 21.- J.A. Otero, O. Mazarrasa, J. Villasante, V. Silva, P. Prádanos, J.I. Calvo, A. Hernández,
54 Three Independent Ways to Obtain Information on Pore Size Distribution of Nanofiltration
55 Membranes, *J. Membrane Sci.* 309 (2008) 17–27.
56
57
58 22.- J.I. Calvo, A. Bottino, G. Capannelli, A. Hernández, Pore Size Distribution of Ceramic UF
59 Membranes by Liquid-liquid Displacement Porosimetry, *J. Membrane Sci.* 310 (2008) 531–538.
60
61
62
63
64
65

- 23.- R. Peinador, J.I. Calvo, P. Prádanos, L. Palacio and A. Hernández, Characterisation of Polymeric UF Membranes by Liquid-Liquid Displacement Porosimetry, *J. Membrane Sci.* 348 (2010), 238–244.
- 24.- R.I. Peinador, J.I. Calvo, K. ToVinh, V. Thom, A. Hernández, Liquid-liquid displacement to characterize retention of virus membranes, *J. Membrane Sci.*, 372 (2011) 366–372.
- 25.- E. Antón, J.I. Calvo, J.R. Álvarez, A. Hernández, S. Luque, Fitting approach to liquid-liquid displacement porosimetry based on the log-normal pore size distribution, *J. Membrane Sci.*, 470 (2014) 219–228.
- 26.- J.I. Calvo, R.I. Peinador, P. Prádanos, L. Palacio, A. Bottino, G. Capannelli and A. Hernández, Liquid-liquid displacement porometry to estimate the molecular weight cut-off of ultrafiltration membranes, *Desalination* 268 (2011) 174–181.
- 27.- A. M. ElHadidy, S. Peldszus, M. I. Van Dyke, Development of a pore construction data analysis technique for investigating pore size distribution of ultrafiltration membranes by atomic force microscopy, *J. Membrane Sci.*, 429 (2013) 373–383.
- 28.- I. N. Hasyimah Mohd Amin, A. W. Mohammad, N. Hilal, Description of membrane fouling characteristics during ultrafiltration of organic foulants contained in sweet water solutions, *J. Environ. Chem. Eng.*, 2 (2014) 1243–1251.
- 29.- R. Kopec, M. Meller, W. Kujawski, J. Kujawa, Polyamide-6 based pervaporation membranes for organic-organic separation, *Sep. Purif. Technol.*, 110 (2013) 63–73
- 30.- PD Sheet - Flat sheet Ultrafiltration membranes – EN.pdf, in <http://www.alfalaval.com/>.
- 31.- Cantor, M, *Uber Capillaritatsconstanten*, *Ann. Phys. (New Foundland)*, 47 (1892) 399–421.
- 32.- L.P. Cheng, H.V. Lin, L.W. Chen, T.H. Young, Solute rejection of dextran by EVAL membranes with asymmetric and particulate morphologies, *Polymer*, 39 (1998) 2135–2142.
- 33.- T. Boccaccio, A. Bottino, G. Capannelli, P. Piaggio, Characterization of PVDF membranes by vibrational spectroscopy, *J. Membrane Sci.*, 210 (2002) 315–329.
- 34.- J.I. Calvo, A. Bottino, G. Capannelli, A. Hernández, R.I. Peinador and R. Firpo, Pore size distribution and MWCO estimations of polymeric membranes by Liquid-liquid Displacement Porosimetry, *Proc. Euromembrane 2009*, Montpellier, France.
- 35.- M. Oldani and G. Schock, Characterization of ultrafiltration membranes by infrared spectroscopy, esca, and contact angle measurements, *J. Membrane Sci.*, 43 (1989) 243–258.
- 36.- N. Giri, R. K. Natarajan, S. Gunasekaran, S. Shreemathi, ¹³C NMR and FTIR spectroscopic study of blend behavior of PVP and nano silver particles, *Arch. App. Sci. Res.*, 3 (2011) 624–630.
- 37.- I. Wienk, Ultrafiltration membrane from polymer blends. Hollow fibers preparation and characterization, PhD Thesis, Twente University, The Netherlands, 1993.

1 38.- S. Munari, A. Bottino, G. Capannelli, P. Moretti, P. Petit-Bon, Preparation and
2 characterization of polysulfone-polyvinylpyrrolidone based membranes, *Desalination*, 70 (1989)
3 265–275

4 39.- A. Hernández, J.I. Calvo, P. Prádanos, L. Palacio, M^a L. Rodríguez, J.A. de Saja, Surface
5 Structure of Microporous Membranes by Computerized SEM Image Analysis Applied to Anopore
6 Filters, *J. Membrane Sci.*, 137 (1998), 89–97
7
8
9

10
11
12
13
14
15
16
17
18
19
20
21
22
23
24
25
26
27
28
29
30
31
32
33
34
35
36
37
38
39
40
41
42
43
44
45
46
47
48
49
50
51
52
53
54
55
56
57
58
59
60
61
62
63
64
65

LEGEND TO FIGURES

- 1
2 Fig. 1.- Typical porosimetric run for a GR70PE membrane.
3 Fig. 2.- Permeability distribution evaluated from data of Fig. 1.
4 Fig. 3.- Pore number distribution obtained by using Hagen-Poiseuille transport model.
5 Fig. 4.- Cumulative distributions of permeability, pore number and pore area, showing the
6 calculation of the Stokes radius used for cut-off estimations.
7
8 Fig. 5.- Porosimetric results: a) porosimetric runs and b) permeability distributions, for
9 several samples of GR61PP membrane
10 Fig. 6.- Porosimetric results: a) porosimetric runs and b) permeability distributions, for
11 several samples of GR70PE membrane
12 Fig. 7.- Cross sectional SEM image of a) GR61PP membrane and b) GR70PE membrane,
13 showing the active layer and macroporous support.
14
15 Fig. 8.- FTIR-ATR spectra of GR membranes as received and after water leaching
16 Fig. 9.- FTIR-PAS spectra of the trunk polymer and additives of GR membrane
17 Fig. 10.- FTIR-ATR spectra of GR70PE membrane before and after LLDP measurements
18 Fig. 11.- Top view SEM image of the active layer of: a) GR61PP and b) GR70PE membranes.
19 Fig. 12.- a) Pore number distributions for GR61PP membrane from LLDP and SEM results; b)
20 Cumulative number distributions for same membrane from LLDP and SEM results,
21 versus MW of a dextran molecule. For the sake of comparison the nominal MWCO
22 value of the membrane is shown as an arrow.
23
24 Fig. 13.- a) Pore number distributions for GR70PE membrane from LLDP and SEM results; b)
25 Cumulative number distributions for same membrane from LLDP and SEM results,
26 versus MW of a dextran molecule. For the sake of comparison the nominal MWCO
27 value of the membrane is shown as an arrow.
28
29
30
31
32
33
34
35
36
37
38
39
40
41
42
43
44
45
46
47
48
49
50
51
52
53
54
55
56
57
58
59
60
61
62
63
64
65

TABLES

Membrane	Porosity / %	r_{pp} / nm	r_{pn} / nm	MWCO / Da
GR61PP				
LLDP-Valladolid	25 ± 6	2.84 ± 0.27	2.42 ± 0.35	19600 ± 2000
LLDP-Genoa	48 ± 10	2.90 ± 0.14	2.03 ± 0.05	21200 ± 3000
Image analysis	$1,54 \pm 0,60$		$2,52 \pm 1.6$	82000 ± 5000
GR70PE				
LLDP-Valladolid	$7,25 \pm 0,70$	6.9 ± 1.3	3.24 ± 0.05	27700 ± 1000
LLDP-Genoa	$9,42 \pm 0,56$	10.7 ± 3.5	3.28 ± 0.83	25600 ± 5000
Image analysis	$1,84 \pm 0,05$		$3,21 \pm 1.0$	65000 ± 4000

Table 1.- LLDP and SEM results of analysis of both membranes.

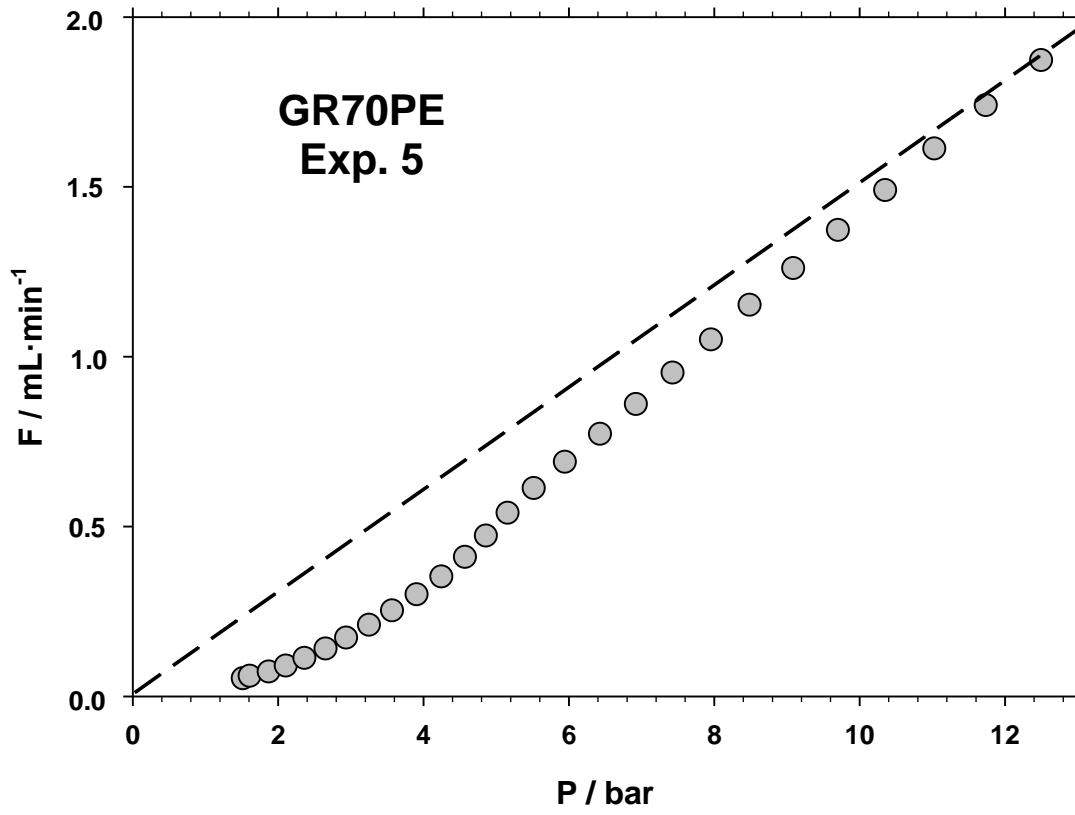


Fig. 1

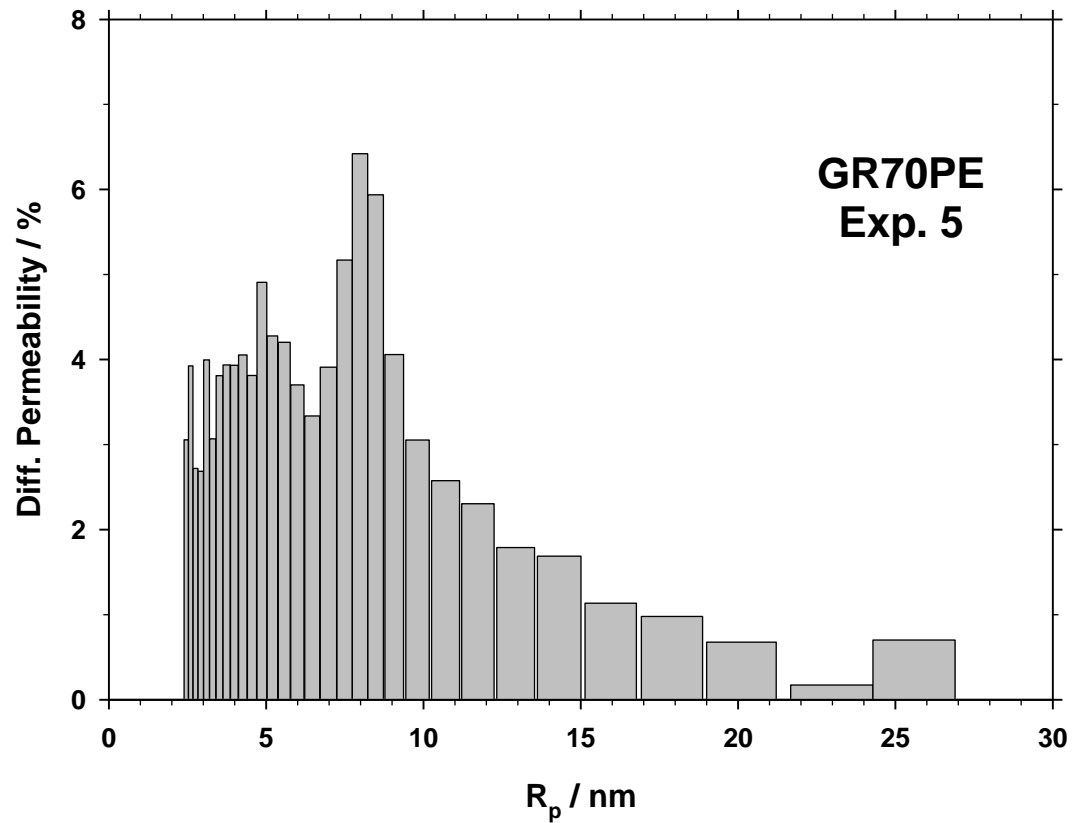


Fig. 2

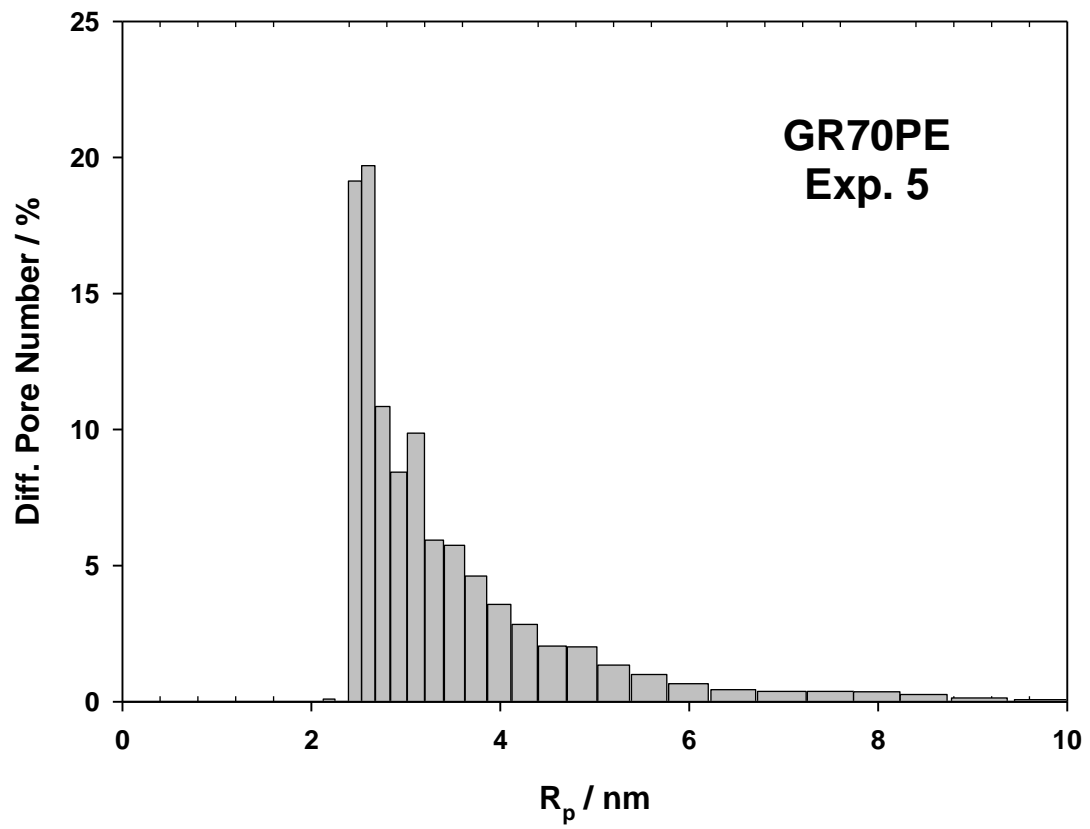


Fig. 3

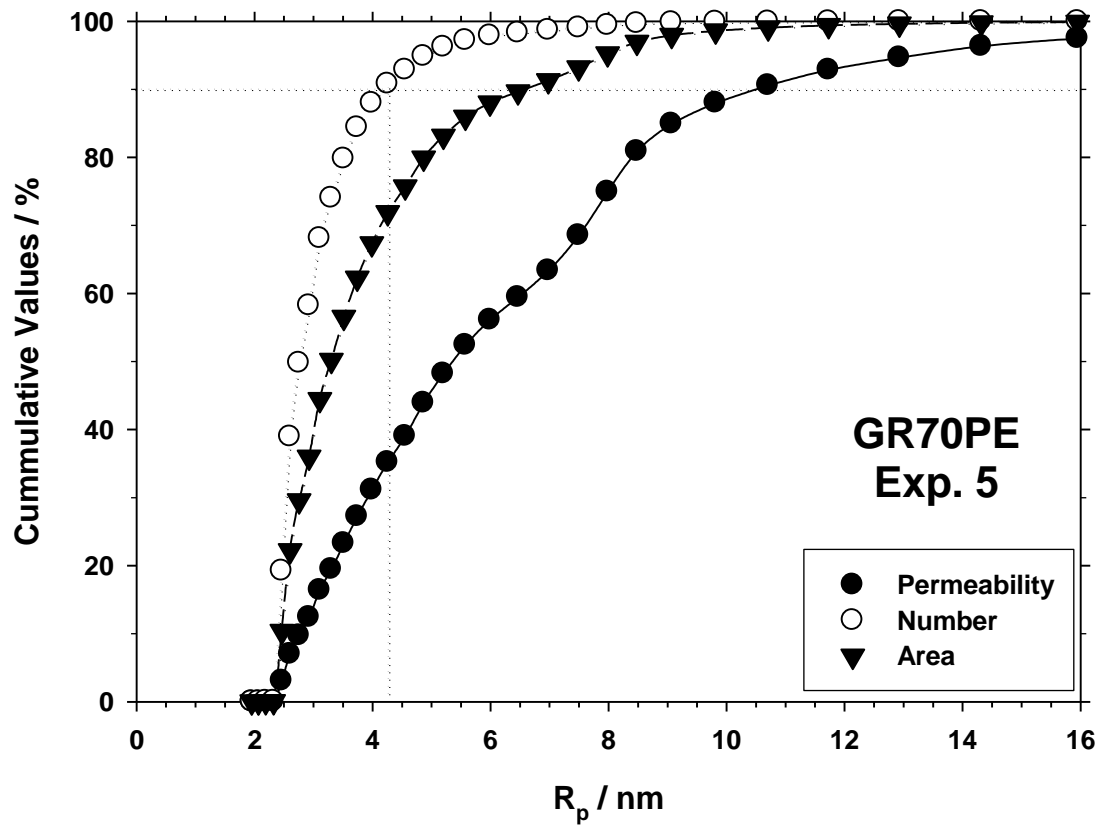


Fig. 4

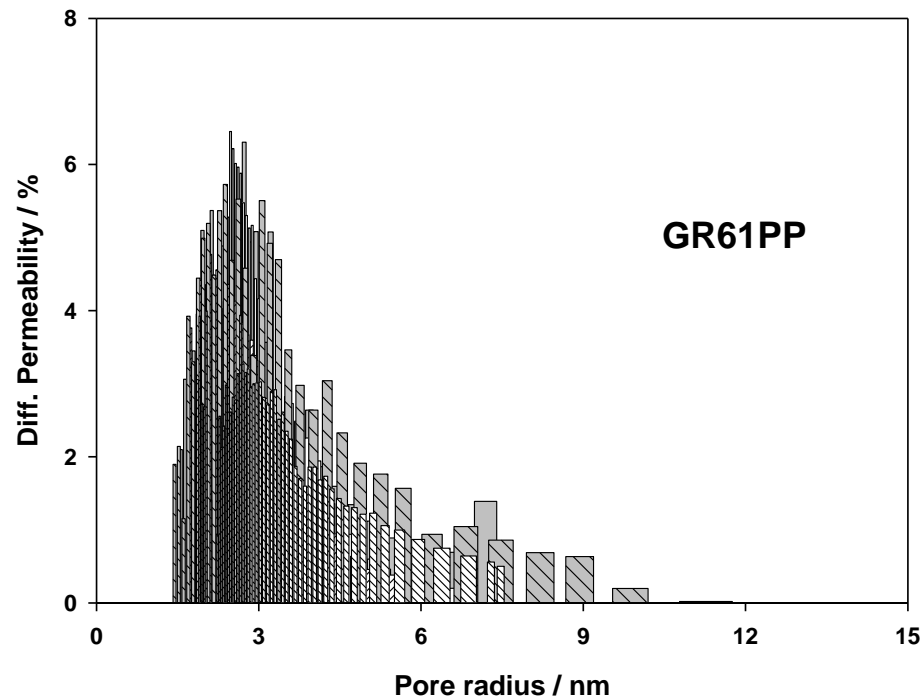
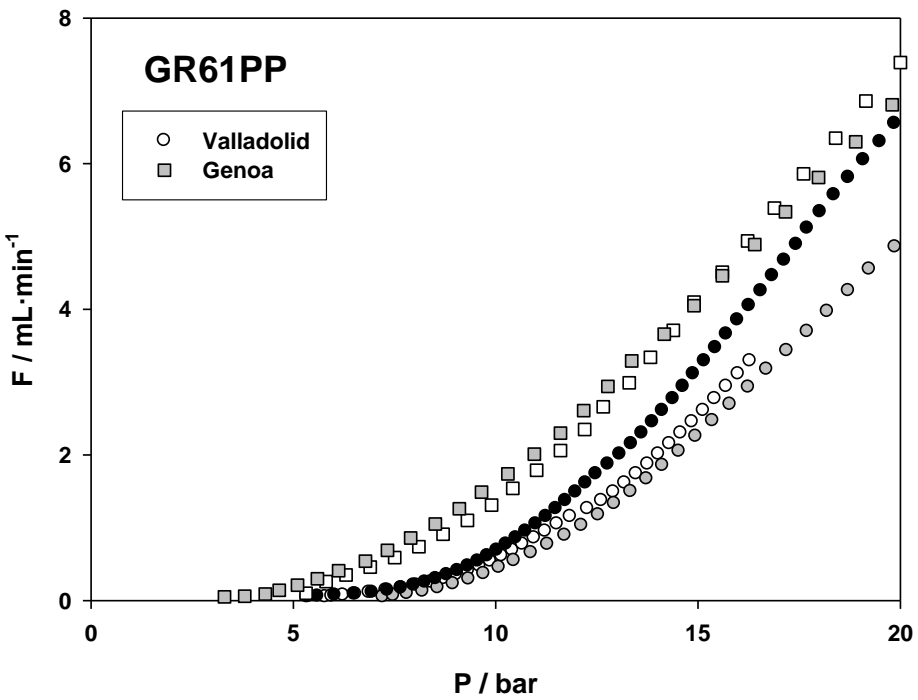


Fig. 5

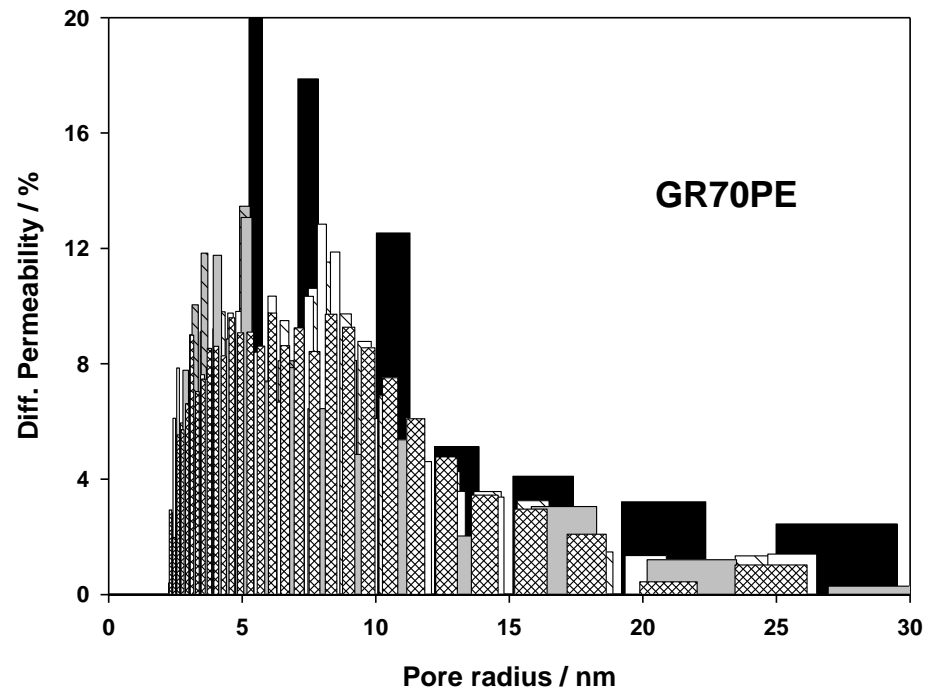
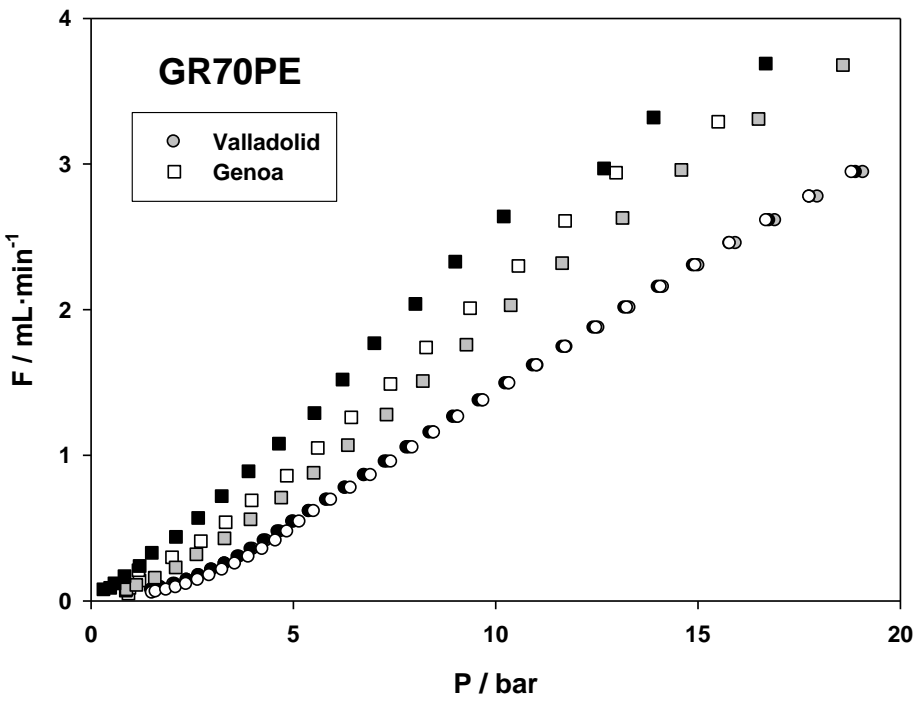
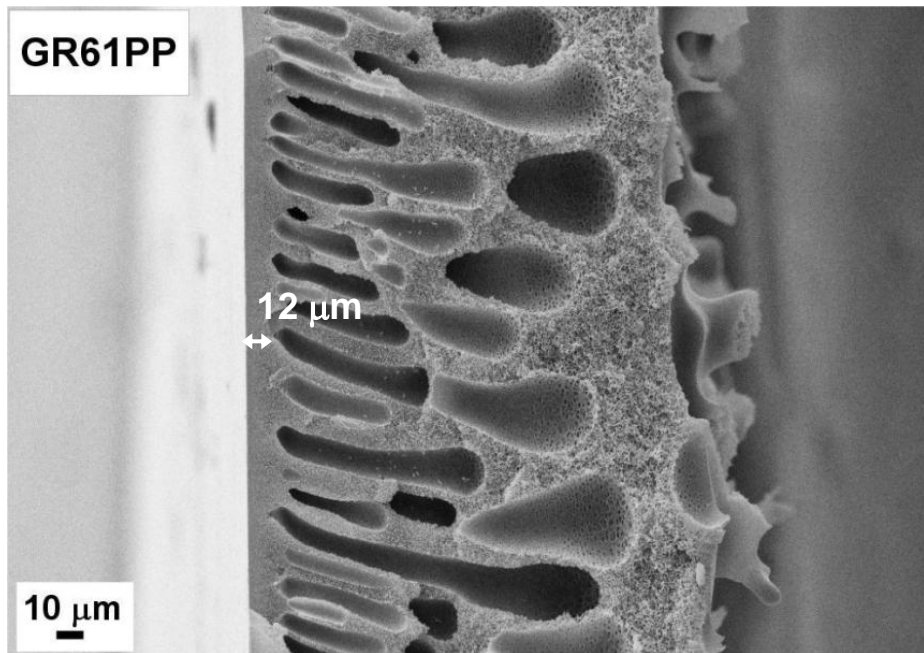
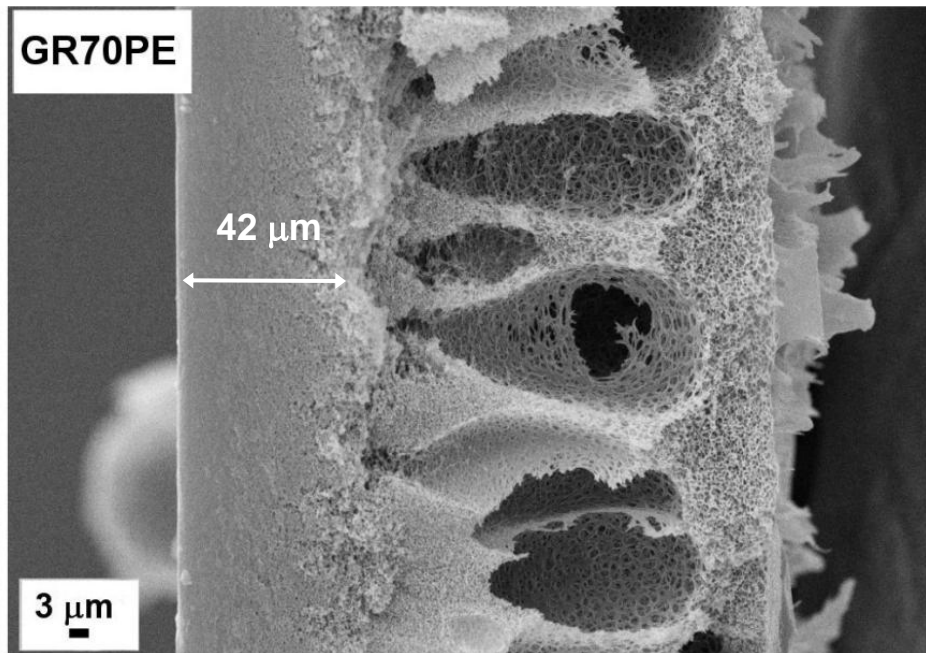


Fig. 6



a)



b)

Fig. 7

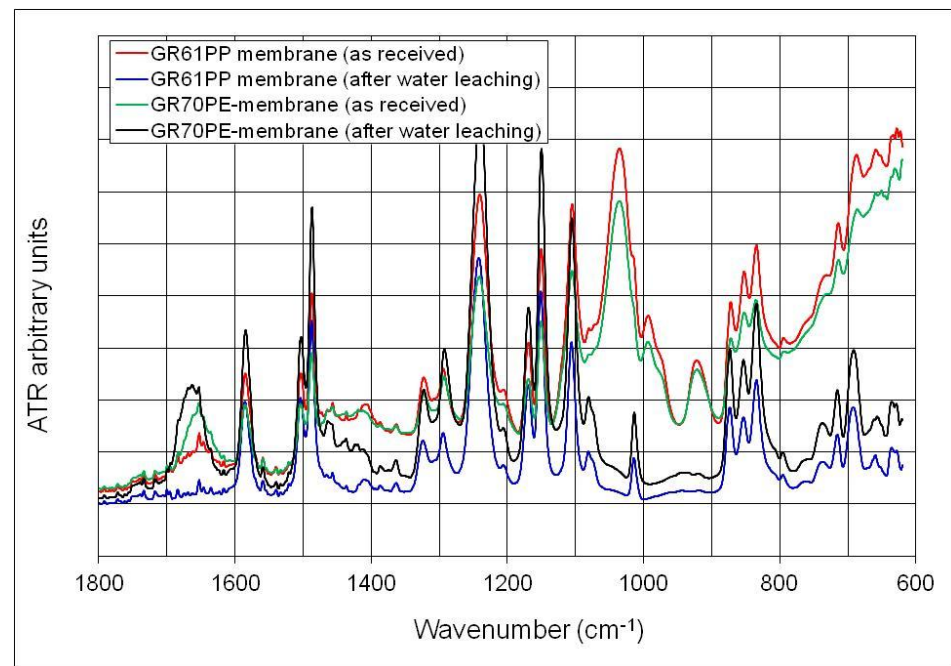
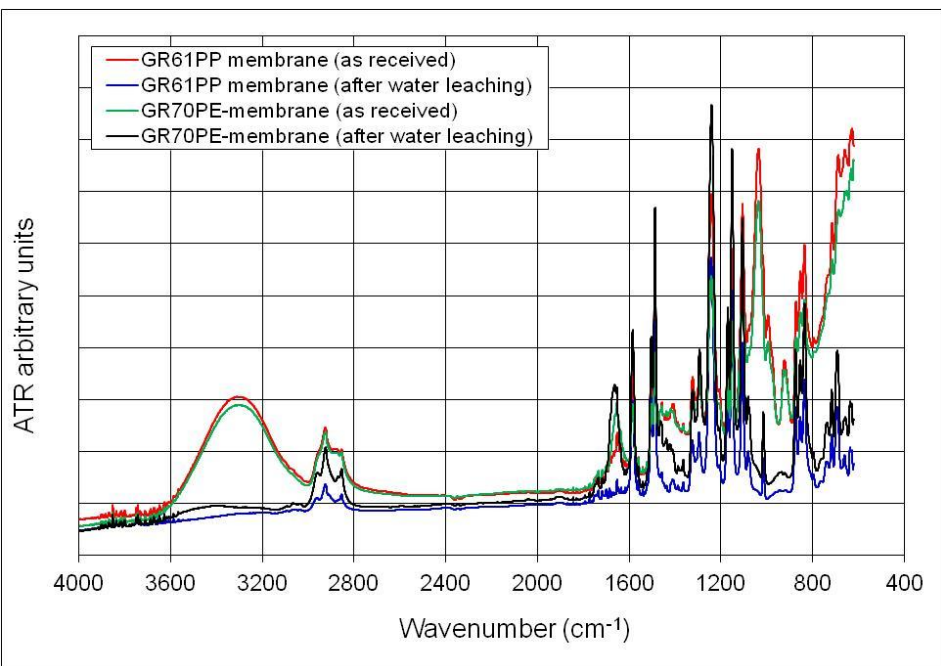


Fig. 8

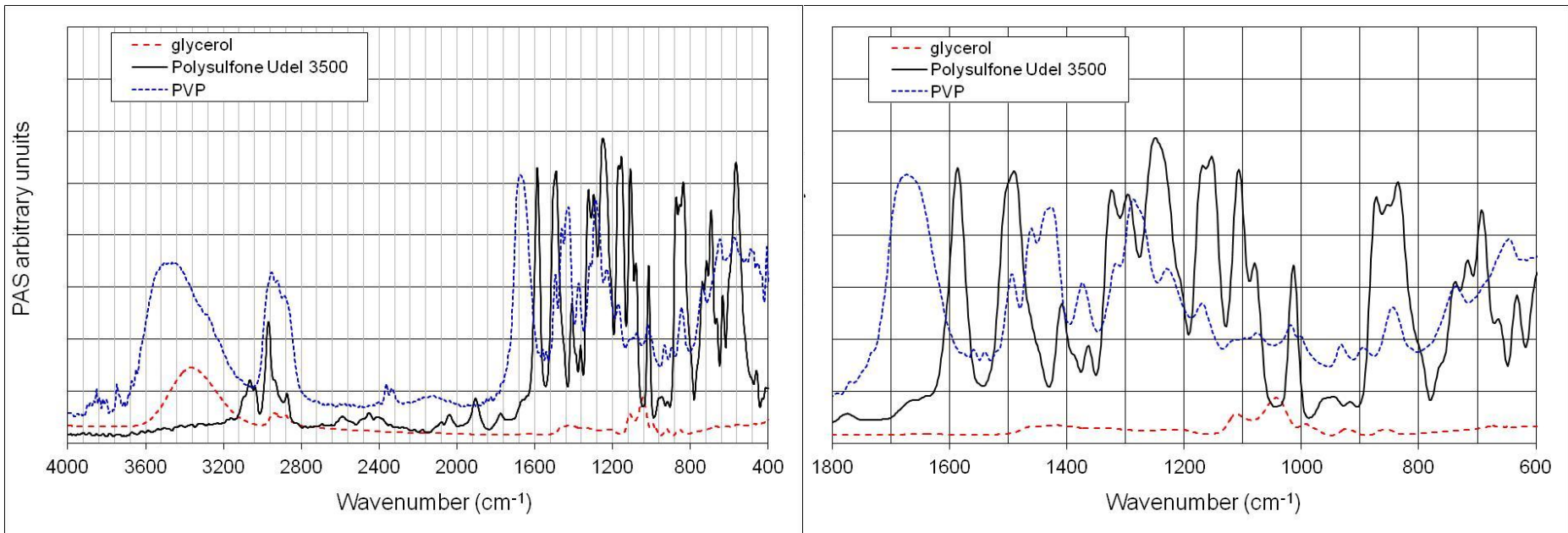


Fig. 9

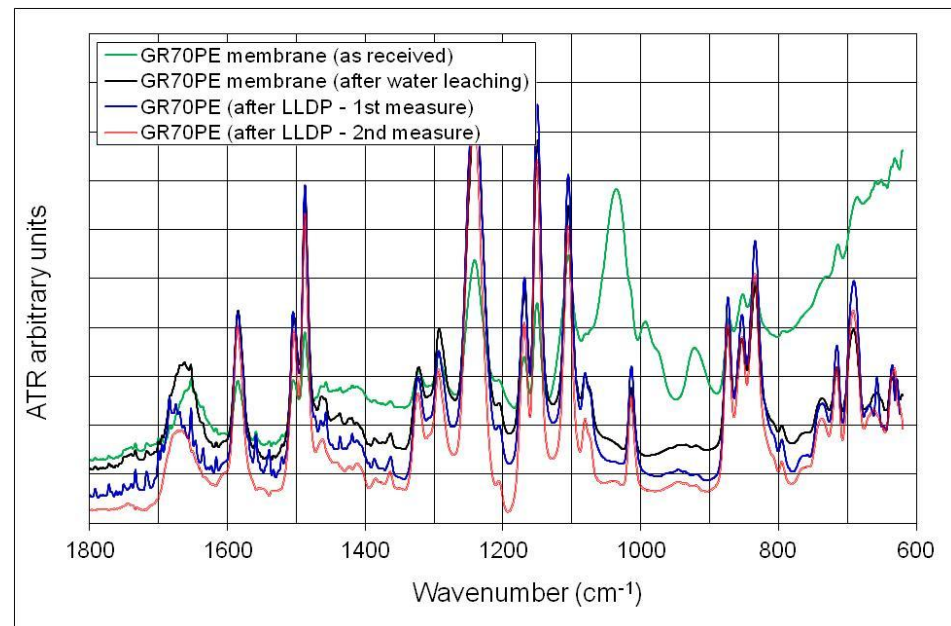
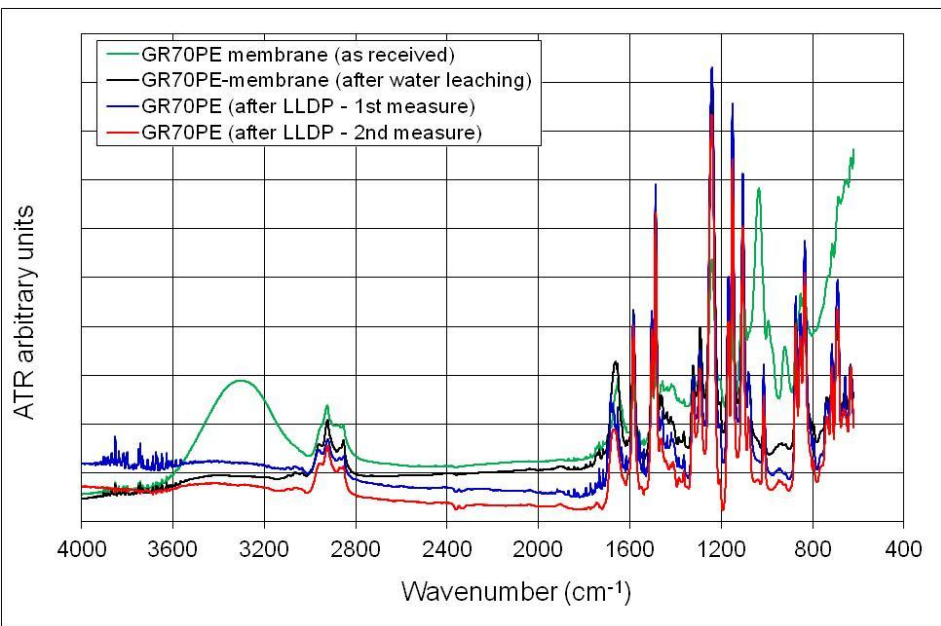


Fig. 10

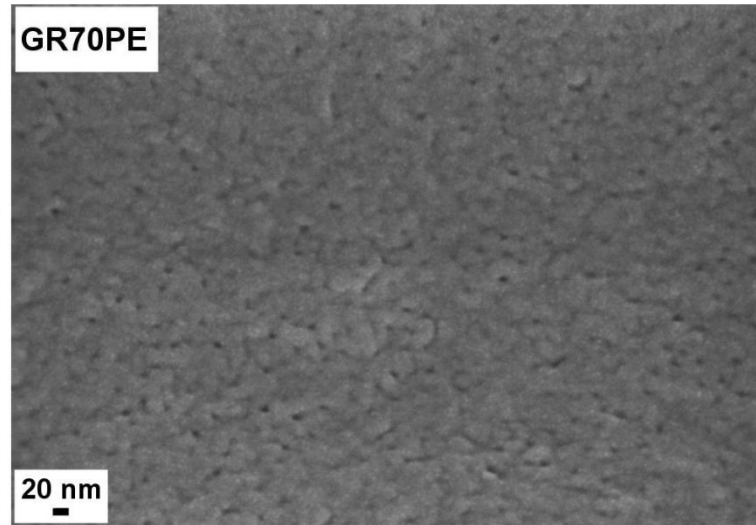
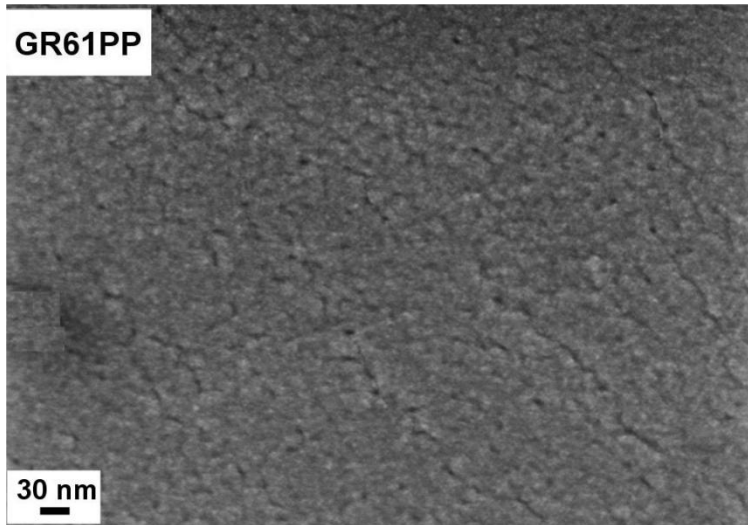
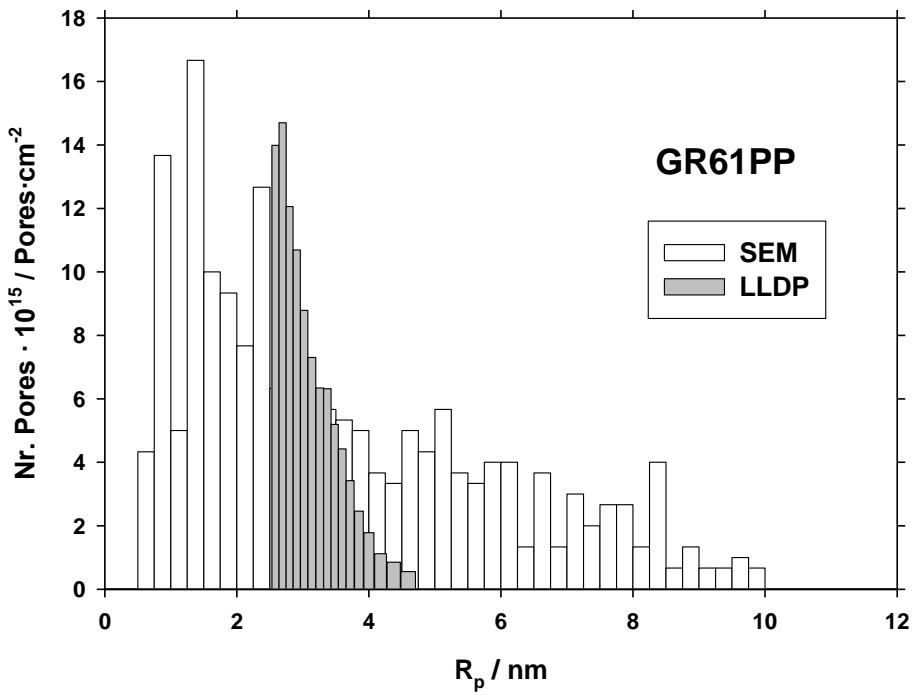
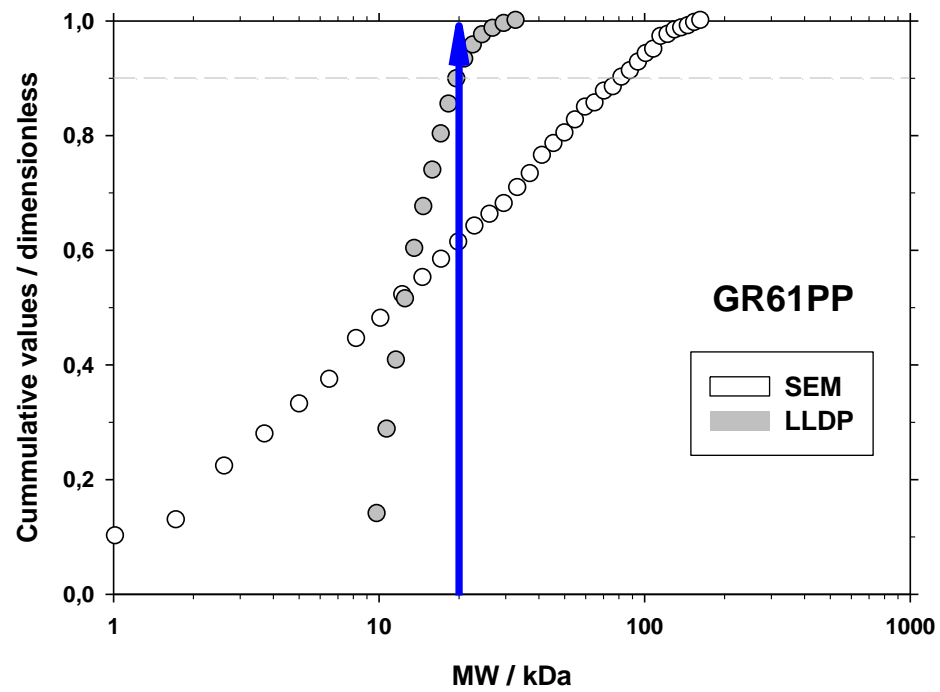


Fig. 11

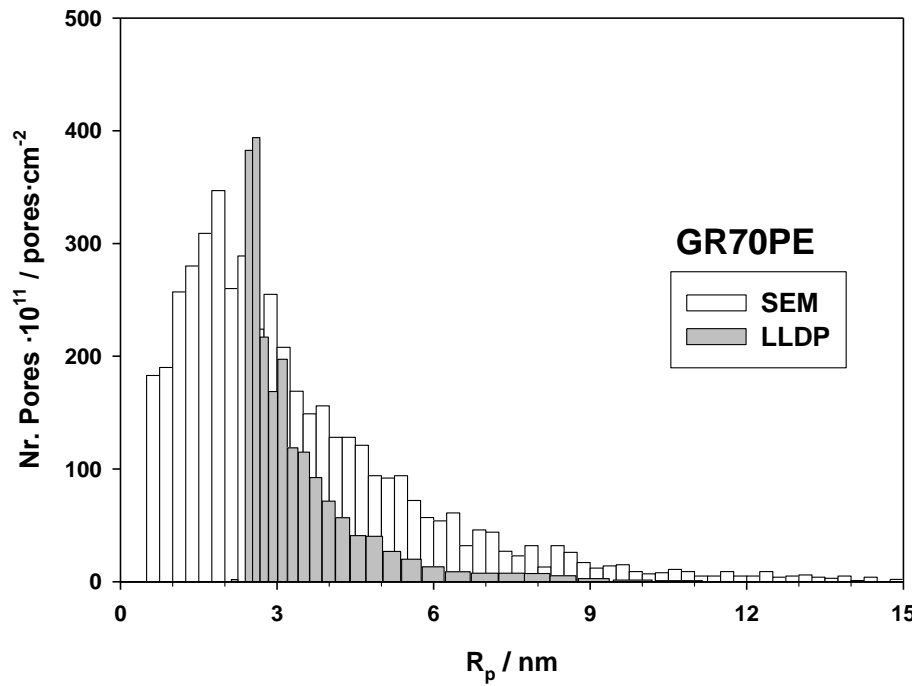


a)

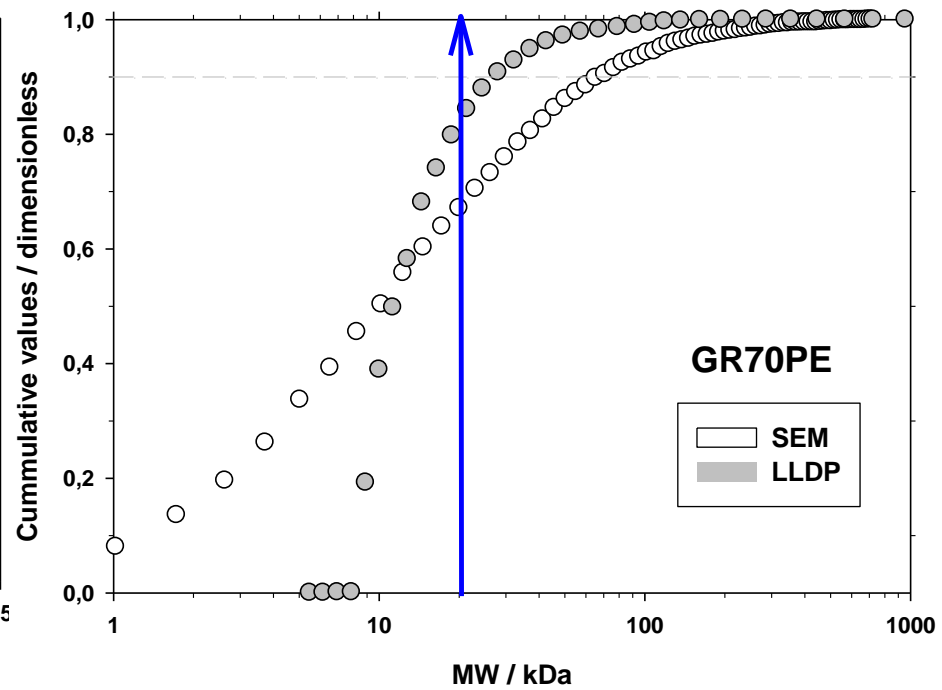


b)

Fig. 12



a)



b)